Proc. Schl. Eng. Tokai Univ., Ser. E
40 (2015) 97-108

Airflow Patterns within Real and 3D Simplified Models of Nasal Cavities (Ⅰ. Experimental Study)

by

Erny AFIZA[*1], Yoko TAKAKURA[*2], Taku ATSUMI[*3] and Masahiro IIDA[*4]

(Received on Mar. 31, 2015 and accepted on Jul. 14, 2015)

Abstract

The human nasal cavity is comprised of complex structures with delicate geometry. Its features make it difficult to simulate the airflow within it, to comprehend the airflow patterns, and to elucidate the roles of the nasal morphology. In this study, in order to clarify the roles and functions in the morphology of each part, realistic and simplified modelling of the human nasal cavity is presented, flow patterns are investigated under steady conditions by in vitro experiments with PIV visualization, and the relevancy of the airflow pattern between two kinds of models is discussed. As the results, flow characteristics for each simplified model were captured and insights into the roles of the morphology of the nasal valve and conchae have been obtained. Furthermore, simplified models with suitable conchae and nasal valves have been proved to be reliable to some extent as similarities can be found between real and simplified models, in the occurrence of swirls at the nasopharynx area and the distribution of flow velocity in the meatus. Thus, complicated phenomena within the real model have been comprehended with the help of simplified models.

Keywords: Nasal cavity, Modeling, In vitro experiment, Particle image velocimetry

1. Introduction

The human nasal cavity is a large, air-filled space extending from the nasal vestibule to the opening of pharynx. As part of the human respiratory system, it is the main conduit for air inspired from the external environment to reach the lungs. The nasal passages have aerodynamic structures lined with mucosal tissue, which act as an air-conditioner to warm and humidify the inhaled air. Besides olfactory function, the short hairs in the nasal vestibule also help prevent harmful materials from entering the lungs. During inspiration, the inhaled air enters the nostrils, passes through the nasal valve[1)] (the narrowest region in the nasal cavity), then flows through the turbinate region before reaching the lungs, where gas exchange takes place.

The aim of this paper is to clarify the functions of the nasal structures through fluid dynamic analysis, focusing on the nasal valve and conchae (turbinates). Nasal surgery is performed without sufficient understanding of the ‘ideal’ nasal airflow, as this is yet to be determined. Therefore, more detailed information on the flow patterns within the human nasal cavity may lead to a better understanding of its physiological functions and improve treatment outcomes.

The nasal valve is located in the anterior region and has the greatest nasal flow resistance because of its small cross-sectional area[2)]. This can cause either disturb or assist the airflow during nasal respiration.

The nasal conchae are the wing-like structures emerging from the lateral nasal walls, covered by mucosal tissue, which are classified into inferior, media and superior conchae. They play an important role in preparing the inhaled air to meet the conditions suitable for entering the pulmonary alveoli. The variation of conchae features among individuals, such as their length, may affect their airflow characteristics and thus the associated physiology[3)].

The influence of intranasal airflow patterns on nasal physiology is indisputable. Excessive resection of the nasal turbinates can cause notable reductions in their air-conditioning performance[4)]. Horschler et al. found in their studies of nasal flows that airflow patterns during inspiration were more susceptible to changes in the natural nasal morphology than during expiration, and concluded that the conchae function as guide vanes to establish a uniform distribution of flow velocity throughout the upper, centre and lower regions of the nasal cavity[5)]. Furthermore, it has been shown that media or inferior turbinectomy can alter the nasal airflow pattern[6)].

There are three main experimental methods for investigating nasal flows: in vivo, in vitro, and in silico. The

*1 Graduate Student, Course of Science and Technology
*2 Professor, Course of Science and Technology
*3 Assistant Professor, School of Medicine
*4 Professor, School of Medicine

most popular form of the latter is computational fluid dynamics (CFD).

In vivo experiments preserve the natural nasal condition, e.g., the properties of the lining tissue, and are thus the most realistic type of experiment. Nonetheless, direct measurements in the human nasal cavity are almost impossible due to the crookedness and narrowness of the geometry. For example, hot wire anemometry obstructs the airflow[7], and the physical contact of the device with the skin and hairs causes a biological reaction. Furthermore, even though experiments in cadavers provide accurate intranasal flow patterns[8], some post-mortem distortion in the nasal geometry due to tissue shrinkage is unavoidable.

In vitro experiments have the advantage of allowing the use of non-invasive methods, such as particle image velocimetry (PIV), which provide more rapid and detailed measurements than the invasive methods used in vivo[9]. In the earliest study, Hopkins et al. used a translucent model and a refractive index-matched working fluid, implanted with particle tracers[10]. High-resolution imaging, such as computed tomography (CT) or magnetic resonance, is required to resolve the anatomical details[11]. CFD has become popular in airway modeling because it avoids many of the difficulties of physical experiments[12][13], and the numerical predictions agree well with PIV measurements[14, 15, 16]. CFD models, however, still require validation against empirical data.

Thus, in vitro experiments were adopted in this study, where the modelling the nasal cavity is inevitable. To our knowledge, up until now, a fully featured physical model of human nasal cavity is yet to be created. Although all models involve simplifications that will cause the results to deviate from the real life situation, accurate predictions are possible even from idealised models. Zhang[17] presented a simplified model of a human nasal cavity that made similar predictions to an anatomically realistic one. Allowing variation in the model geometry is desirable to account for the natural differences in nasal geometry between individuals, which is attributed to, amongst other things, climatic adaptation and genetic materials. In other words, the predicted airflow pattern in one model will only provide limited information, even if it is obtained from a perfectly realistic model[11]. However, as simplified models are amenable to making variations in the geometry, such as the removal and addition of features, they are useful for studying the relationship between airflow patterns and structural changes in the nasal cavity. In the present paper, to interpret the flows within the human nasal cavity, simplified models[18][19] are designed and the flow patterns are compared with those of an anatomically realistic model[3].

In previous studies, the authors investigated flow patterns in pseudo two-dimensional (2D) models[3, 15, 20, 21]. It was found that the conchae play a role as guide plates to prevent large-scale reverse flows within a nasal cavity, and that the length of conchae determines the airflow distribution in the three meatuses; the longer media concha makes the flow pass the media meatus. Following on, simplified 3D models were developed, which consisted of the common meatus and 3D turbinates inside a pseudo-2D cavity model, to approximate the real anatomy[22]. The simplified 3D models produced more realistic flow patterns than their 2D predecessors.

In the present research, as extensive study, the airflow pattern in 3D models are discussed in detail. The effects of variation in nasal morphology, such as conchae and nasal valve, in simplified models are investigated in attempt to clarify its morphologic roles and functions physiologically.

2. Experimental Setup

2.1 *Model Creation*

In this study, we created two types of human nasal cavity model: anatomically realistic and simplified. The anatomically realistic model was derived from a high-resolution CT scan of a Japanese adult. In the simplified models, the passageway in the nasal cavity was intentionally truncated, leaving only the main parts.

2.1.1 *Anatomically Realistic Model*

A highly detailed physical model of the human nasal cavity was fabricated in collaboration with Tokai University Hospital and Sony Corporation, shown in Fig. 1. This 3D model was reconstructed from high-resolution CT images, having a spatial resolution of 512×512 pixels and a 0.3-mm slice width. These data were converted into an AutoCAD file and the physical model was fabricated from silicone by the salt deposition method.

We did not consider anatomical variation between the two nasal cavities and therefore only modeled one nasal cavity. We also neglected nostril hairs, external nose shape and the properties of nasal tissues, such as their moisture and temperature. Figure 1(a) and (b) show the front and side views of the human nasal cavity, respectively. Figure 3 is a midline sagittal section (Fig. 1(c)) of the model showing the distribution of the cross-sectional area (CSA). The smallest area, which is located at 15 mm from the nostril, denotes the nasal valve.

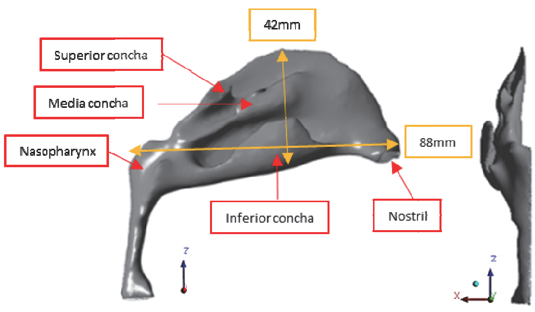

(a) Front view (left) and side view (right)

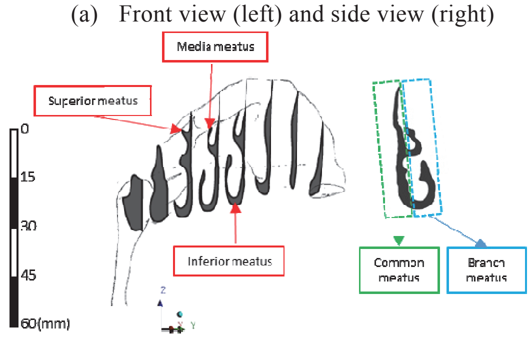

(b) Cross-sectional area

Fig. 1 Human nasal cavity model

2.1.2 *Variation of Simplified Models*

In a previous study, we built quasi-2D simplified models of the human nasal cavity that consisted of a media concha and an inferior concha, using a transparent acrylic plate[3]. In the present paper, we built simplified 3D models that also included the common meatus and the turbinates but omitted the superior concha, assuming it to be comparatively less important to the airflow pattern. Curves were also added to both ends of conchae area. In these models, the cavity length and width were 90 mm and 10 mm, respectively, giving a nasal ratio (cavity length/cavity height) of 2.3.

Six models (A–F) were designed, shown Fig. 2(a); their hydrodynamic descriptions are given in Table 1. Model B was designated to be the standard model. We investigated how the following modifications affected the airflow pattern:

(a) Without any conchae (Model A)

(b) Variation of the length of the media concha (Models B and C). In Model C, the length of the media concha was shortened by dissecting the anterior and posterior parts of the concha in Model B. The concha was placed in the middle of the media region for both cases.

(c) The presence of either the media or inferior turbinates. Only one turbinate was investigated in each model (Models D and E).

(d) The addition of the nasal valve to model B (Model F). To mimic the nasal valve, a constriction was added near the nostril with a minimum hydraulic diameter of 7 mm.

Figure 3 shows the distribution of the CSA in the anatomically realistic and simplified models. The CSA profile in the anatomically realistic model is similar to the typical CSA profile of a nasal cavity in Doorly et al.[12]. The local minimum in cross-sectional area in the anatomically realistic model and in Model F, which is located 15 mm from the nostril, corresponds to the nasal valve.

2.2 *Experimental Methods*

We used PIV to obtain the instantaneous 2D velocity field, as shown in Fig. 4 (left). A laser sheet was projected throughout the model in the main tank. Figure 4 (right) is a schematic diagram of the experimental apparatus, which includes a circulating flow system connected to the model in the tank. A pump is attached to the nasopharynx of the model to simulate steady continuous respiratory flow.

In the anatomically realistic model, the airflow pattern was visualised using a solution of glycerol (48 wt%) and water (52 wt%) as the working fluid and Orgasol polyamide powder (Arkema group) as the tracer. Glycerol is a clear, colorless fluid, and has the highest refractive index of all water-soluble materials. It was used to match the refractive index of the (anatomically realistic) silicone model to prevent laser sheet deflection. For the simplified models, tap water was used as the working fluid (with the same tracer). Experiments were carried out over the range of Reynolds numbers that correspond to average healthy Japanese people at typical resting breathing rates: Re = 880–1530[23]. Reynolds number was defined by using the hydraulic diameter and flow velocity at the nostril area (outlet). From continuity equation, flow velocity at the trachea was derived which is set to be the inlet.

Table 1. General features of the simplified 3D models

Model	Features	Media meatus length (mm)	Inferior meatus length (mm)
A	Without conchae	-	-
B	Long-media concha	48	48
C	Short-media concha	29	48
D	Media concha only	48	-
E	Inferior concha only	-	48
F	Model B+nasal valve	48	48

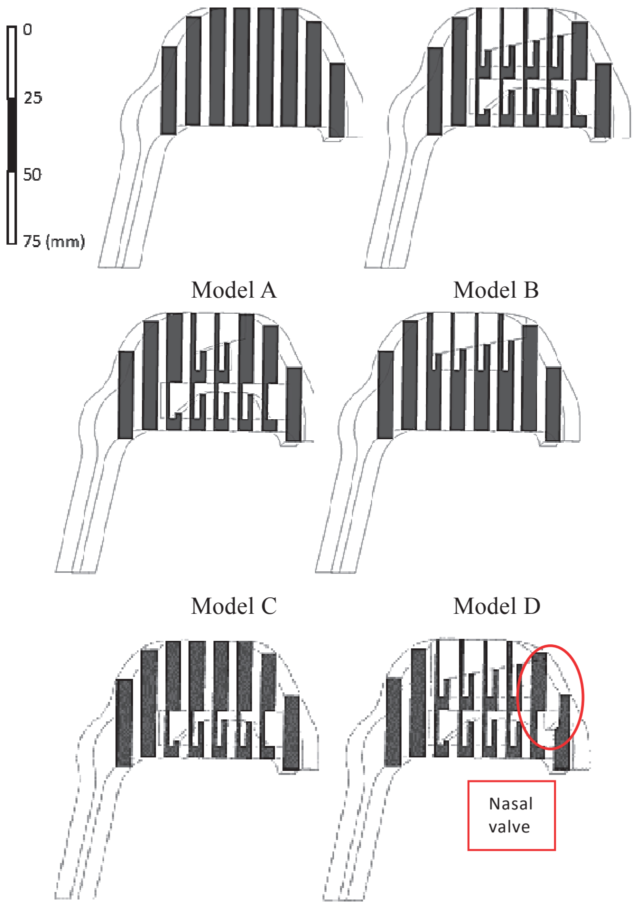

(a) Cross-sectional area

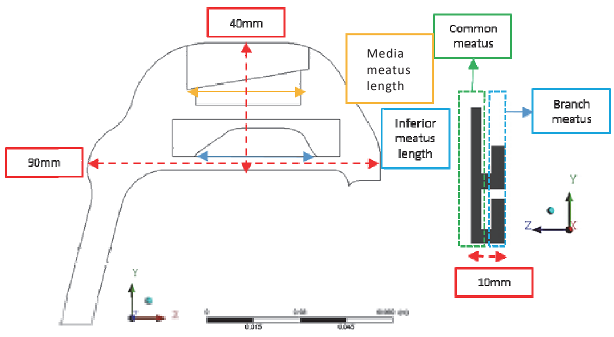

(b) Measurement and partial definition

Fig. 2 Simplified Models of the human nasal cavity

Table 2 Experimental setup for inspiratory and expiratory flows in the anatomically realistic and simplified models

Model	Working fluid	Reynolds number	Flow velocity at trachea (m/s)	Hydraulic diameter at nostril (mm)	Kinematic viscosity (m^2/s)	Temperature (°C)
Real	water solution of glycerol	880	1.28	5.76	4.83 x10^{-6}	20
Simplified	water	880	0.46	5.7	1.004x10^{-6}	20

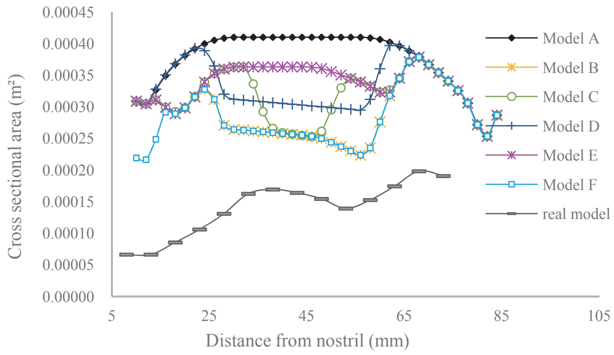

Fig. 3 Distribution of cross-sectional area along the nasal cavity in the simplified 3D models

As almost no differences were observed in the flow patterns in this Reynolds number range, we only present the Re = 880 results. The dimensions of the anatomically realistic and simplified models are shown in Table 2.

3. Results

3.1 *Anatomically Realistic Model*

The path lines during 0.06s along the wall in the meatus and streamlines in the anatomically realistic model (main nasal passage: common meatus; superior, media, and inferior meatus: branch meatus) during inspiration and expiration are presented in Figs. 5 and 6, respectively. The characteristics of flow patterns are as follows:

(1) During inspiration (Fig. 5), the highest velocity is recorded in the media meatus. In the common meatus, the flow jets in the middle region, a large 3D whirl is detected in the superior region near the olfactory area, and small-scale swirls occur in the upper region near the nasopharynx and in the opening of the inferior meatus.

(2) During expiration (Fig. 6), the highest velocities occur in the middle and inferior regions of the common meatus and in the media meatus. The flow velocity is more uniform at the entrance of all meatuses than in inspiration. In the superior region of the common meatus the velocity magnitude is very small, and as in the inspiration results, small-scale swirls are observed in the upper side of nasopharynx and in the opening of the inferior meatus.

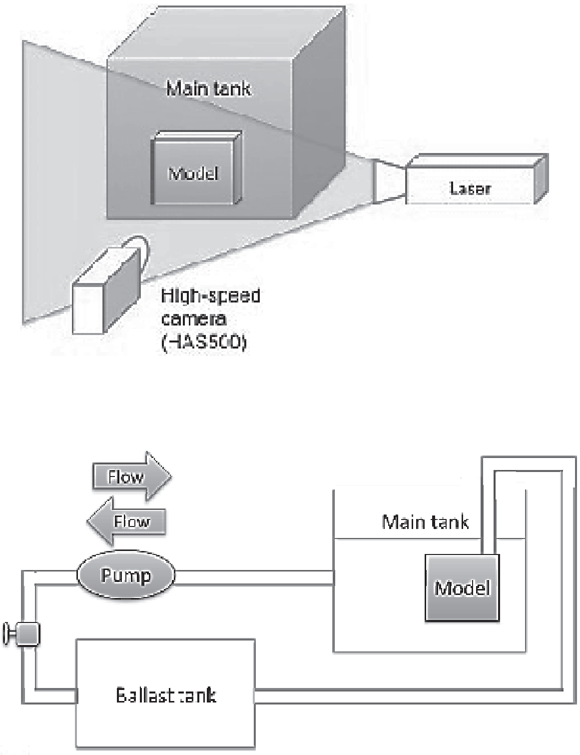

Fig. 4 Schematic of the PIV apparatus (top) and overall rig (bottom)

3.2 *Simplified Model: Without Conchae*

3.2.1 Inspiration

Figure 7 shows the path lines during 0.06s along the wall in the meatus and streamlines during inspiration for Model A (without conchae). The bulk of the airflow occurs in the superior region of the nasal cavity (between the nostril and nasopharynx), guided by shape of the nasal cavity. A large-scale whirl is found in the centre where the conchae are normally located. Due to an abrupt change in the geometry at the posterior airway passage, a small swirl is detected near the nasopharynx opening.

3.2.2 Expiration

During expiration in Model A (Fig. 8), the high flow rate causes the airflow to deflect at the nasopharynx opening and bypass the upper side of the airway. As in the inspiratory flow, the absence of conchae induces the formation of a large whirl in the centre of the cavity and a small swirl occurs at the posterior side near the nasopharynx.

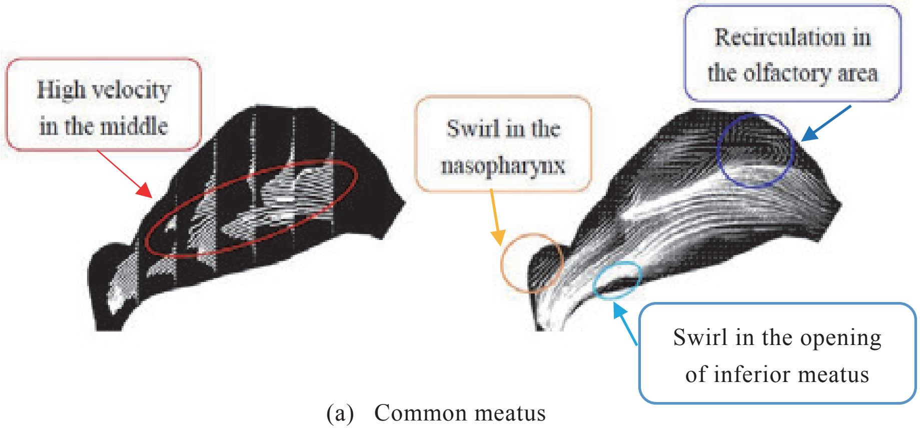

(a) Common meatus

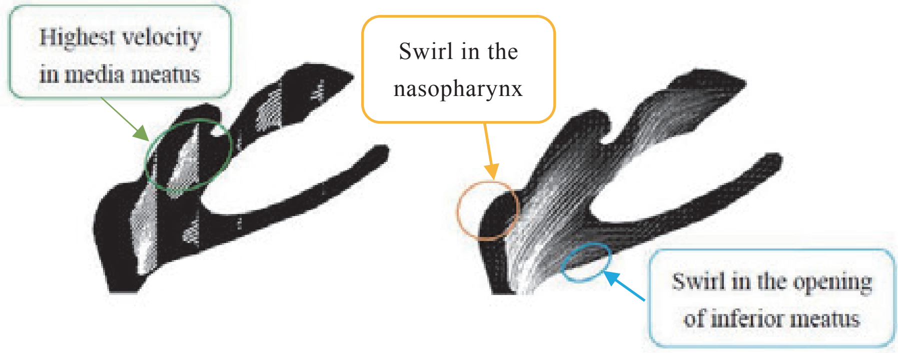

(b) Branch meatus

Fig. 5 Pass lines and streamlines during inspiration

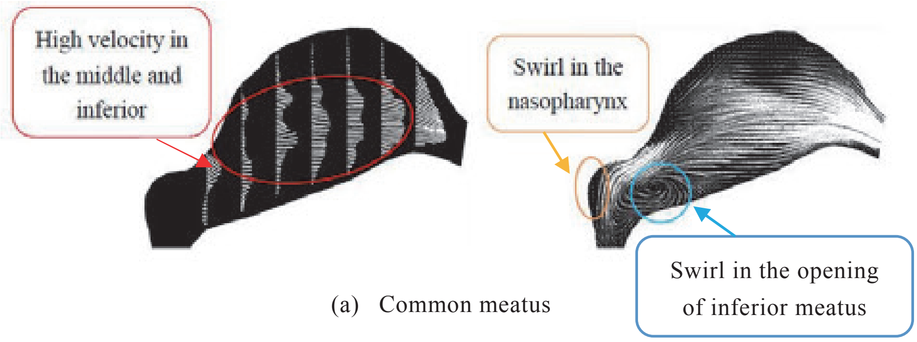

(a) Common meatus

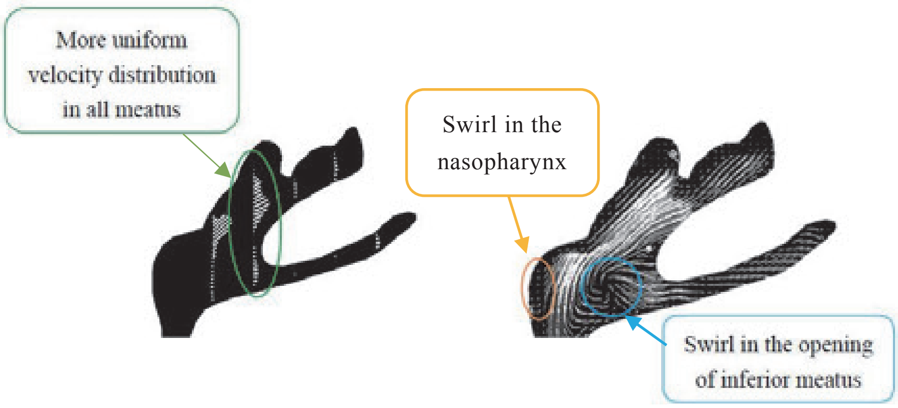

(b) Branch meatus

Fig. 6 Pass lines and streamlines during expiration

3.3 *Simplified Models: Different Length of Media Concha and Presence of Nasal Valve*

3.3.1 Inspiration

Figure 9(a) and (b) show the path lines during 0.06s along the wall in the meatus and streamlines during inspiration in the simplified 3D models. In the common meatus (Fig. 9 (a)), almost no difference in the airflows can be observed between models B and C, which have different length of media concha. High flow rate is detected in the middle and superior regions and swirl occurs at the anterior side of the nose, accompanying slow reversed flow in the inferior region (Fig. 9 (a) and (b)). By comparing Fig. 7 and Fig. 9(a), it is clear that the conchae reduce size of the whirl. Furthermore, the presence of the nasal valve (Model F) prevents the whirl from occurring. From the streamlines results, we see that small-scale swirls occured at the upper side of nasopharynx area in all models, similar to the results for the anatomically realistic model.

The visualisation results of the branch meatus (Fig. 9(b)) show that flow velocity is higher in the media meatus in the models with a long media concha (Model B) and with a nasal valve (Model F), compared with that in the model with a short media concha (Model C). The long media concha guides the flow into the media meatus.

3.3.2 Expiration

As shown in Fig. 10(a), while exhaling, the airflow distributes almost uniformly along the cavity in the common meatus in Models B and C. With the presence of a long media concha and a nasal valve (Model F), however, the airflow is slow in the superior region of the common meatus, which also can be seen in the anatomically realistic model (Fig. 6(a)). Medium-scale swirls are observed near the nasopharynx area and at the opening of the inferior region of all models, which agrees with the results of the anatomically realistic model. The average velocity magnitude in the media meatus is larger than that in the inferior meatus in all cases (Fig. 10(b)). Furthermore, it is noted that the flow is introduced from the common meatus to the middle of inferior meatus in all models, which also can be confirmed by using numerical simulation for the real model [15, 24)]. In all models, main passageway of the airflow for branch meatus is the media meatus

3.4 *Simplified Models: Presence of Media or Inferior Concha Only*

3.4.1 Inspiration

Without the presence of the inferior concha (Model D) in Fig. 11(a), the large whirl in the centre (as in Model A) causes the airflow to concentrate in the upper region, and reversed flows are detected where the inferior concha would otherwise be located in the common meatus. When the inferior concha was the only flow structure (model E), the airflow pattern in the common meatus, which was predominantly in the superior and middle regions, was almost indistinguishable from that in the two models with both conchae (Models B and C, Fig. 9 (a)).

From Fig. 11(b), we see that with the media concha only (Model D), the flow concentrates in the middle meatus, which also can be seen in the models with both conchae (e.g., Model B in Fig. 9 (b)). High-speed flow is detected in the superior region in with the inferior concha only (Model E). In the streamline results, small-scale swirls are detected at the nasopharynx area in both models (Model D and E).

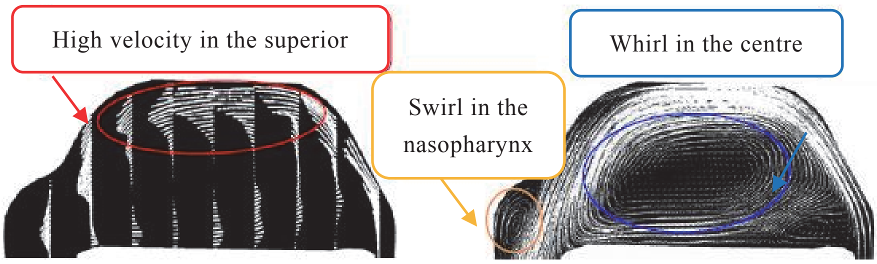

Fig. 7 Pass lines and streamlines during inspiration

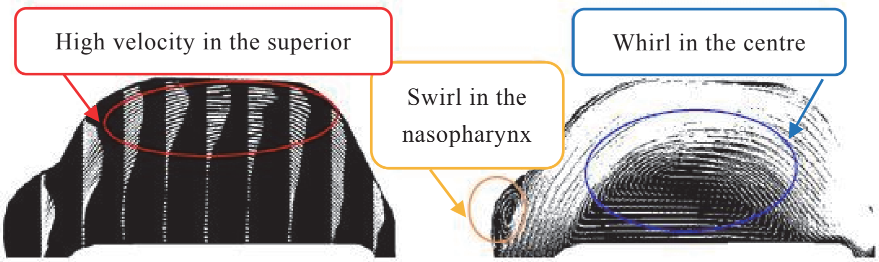

Fig. 8 Pass lines and streamlines during expiration

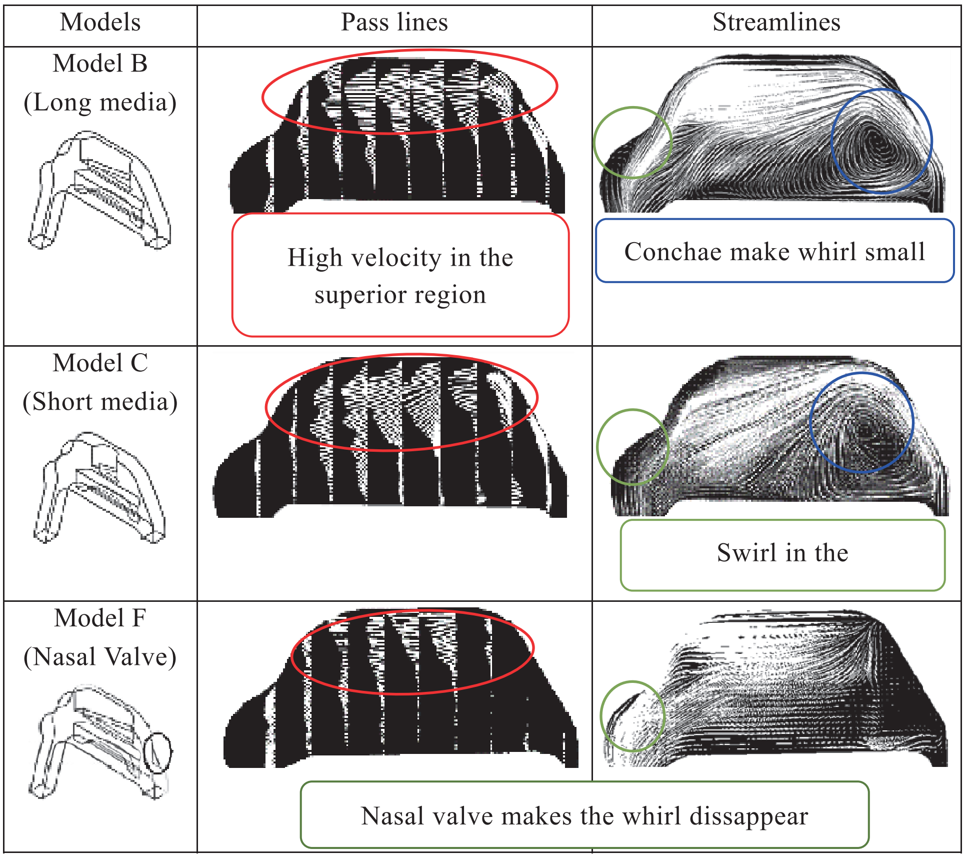

(a) Common meatus

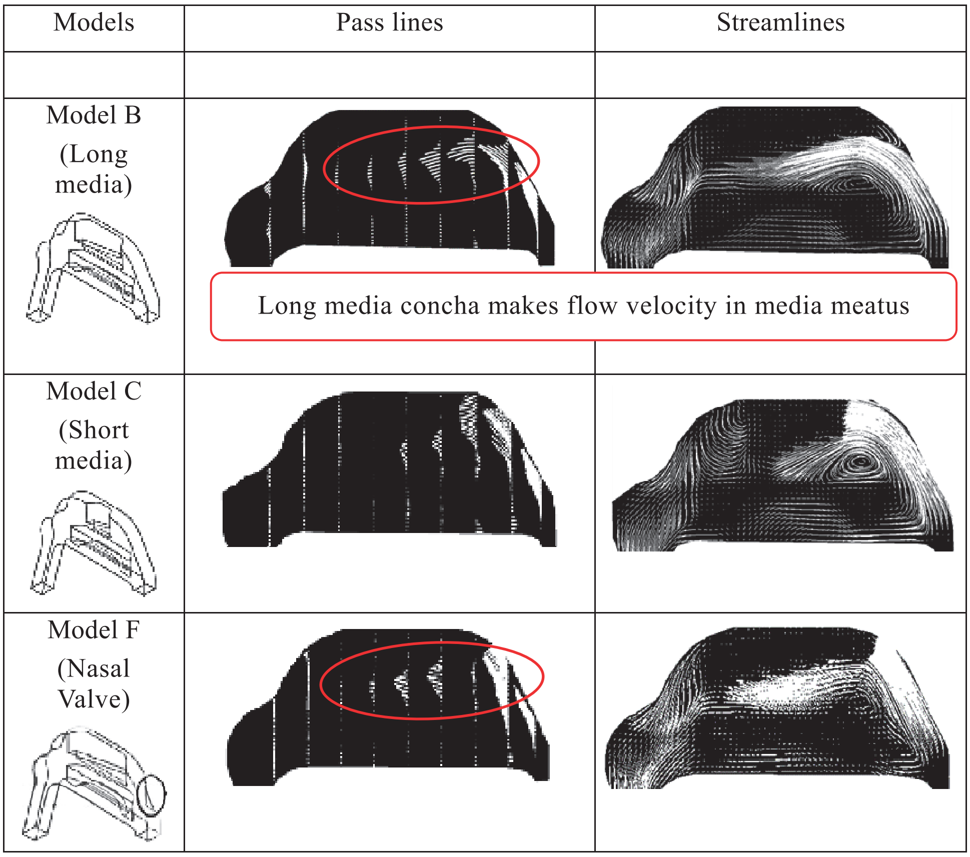

(a) Branch meatus

Fig. 9 Pass lines and streamlines during inspiration

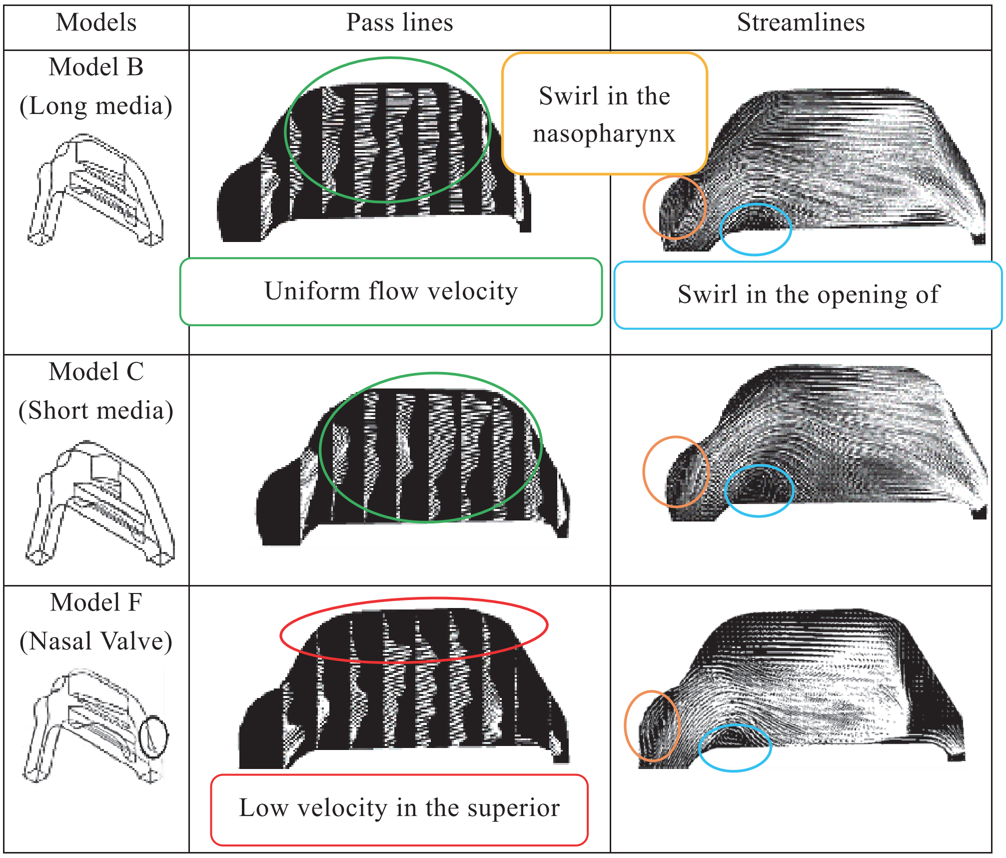

(a) Common meatus

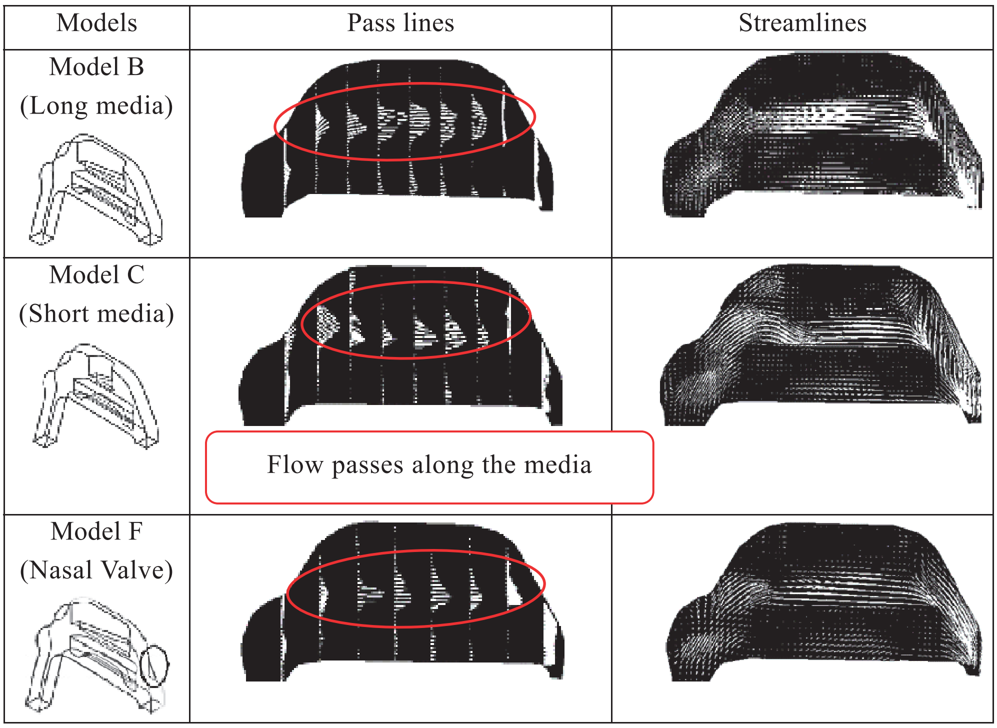

(b) Branch meatus

Fig. 10 Pass lines and streamlines during expiration

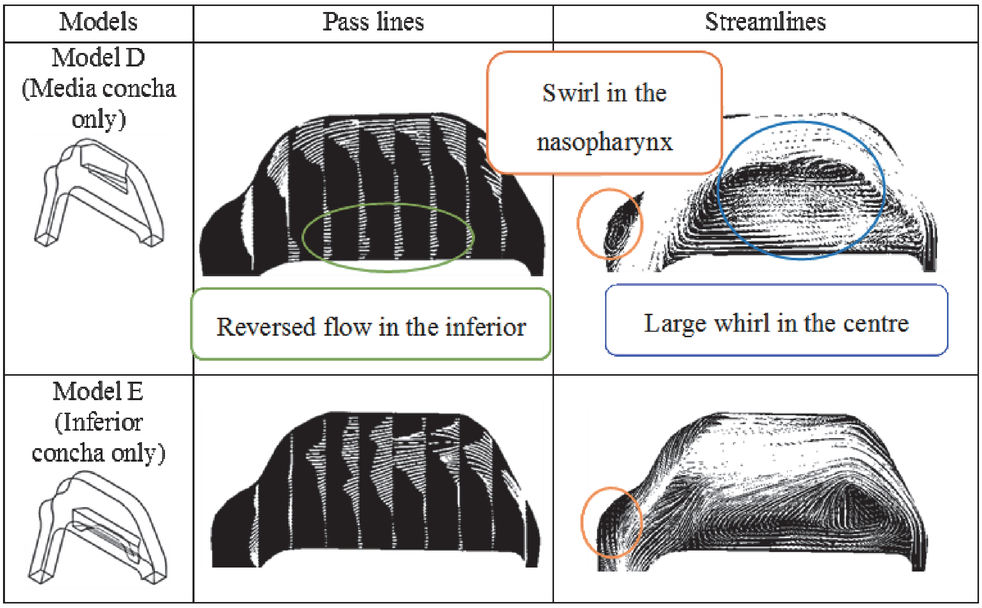

(a) Common meatus

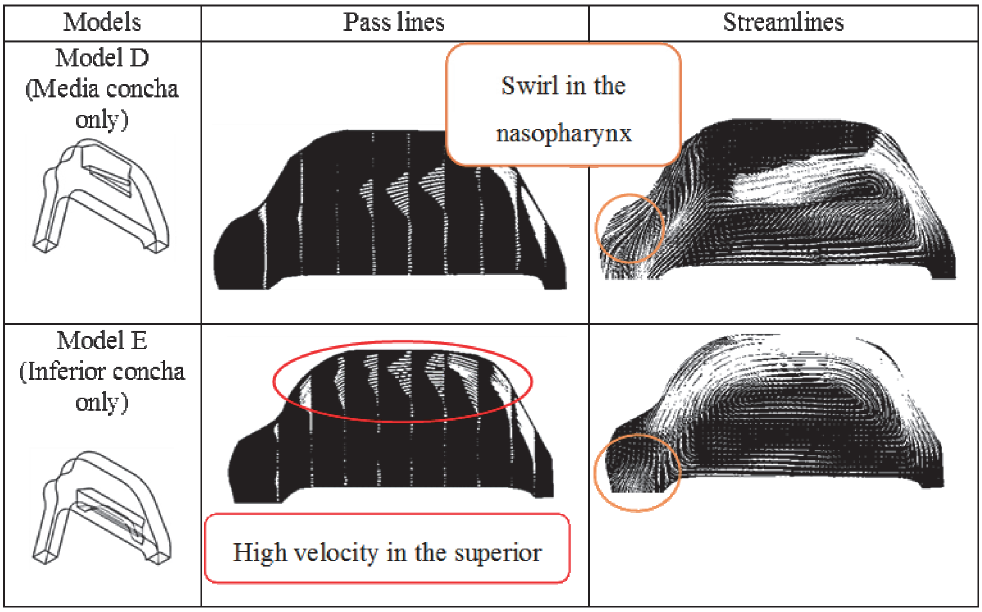

(b) Branch meatus

Fig. 11 Pass lines and streamlines during inspiration

3.4.2 Expiration

During expiration in Model D, which lacks the inferior meatus, the flow is fastest in the upper region (Fig. 12(a)). In Model E, despite the absence of the media concha, the airflow distributes almost uniformly, which also is observed in models with both conchae (Models B and C, Fig. 10(a)). This suggests that the inferior concha acts to distribute the flow evenly within the common meatus. Swirls occur near the nasopharynx in models D and E, the same result as for inspiration.

In Fig. 12(b), high-speed flow is observed in the position where the inferior or media concha would otherwise be located: in the medial region in Model D and in the superior region in Model E

4. Discussion

We now discuss the similarity of the airflow patterns between the anatomically realistic and simplified models to determine the roles of each nasal structure.

4.1 *Inspiration*

We begin with the simplified models. In Model A, without the presence of either conchae, a large-scale whirl occurs in the middle of the nasal passage. In the models with conchae, swirls occur on a smaller scale in the common meatus, which accompanies slow reversed flow in the inferior meatus in Models B and C, but not in Model F. These results suggests that the conchae act as guide plates to reduce the size of the recirculation region, which is aided by the presence of the nasal valve (Model

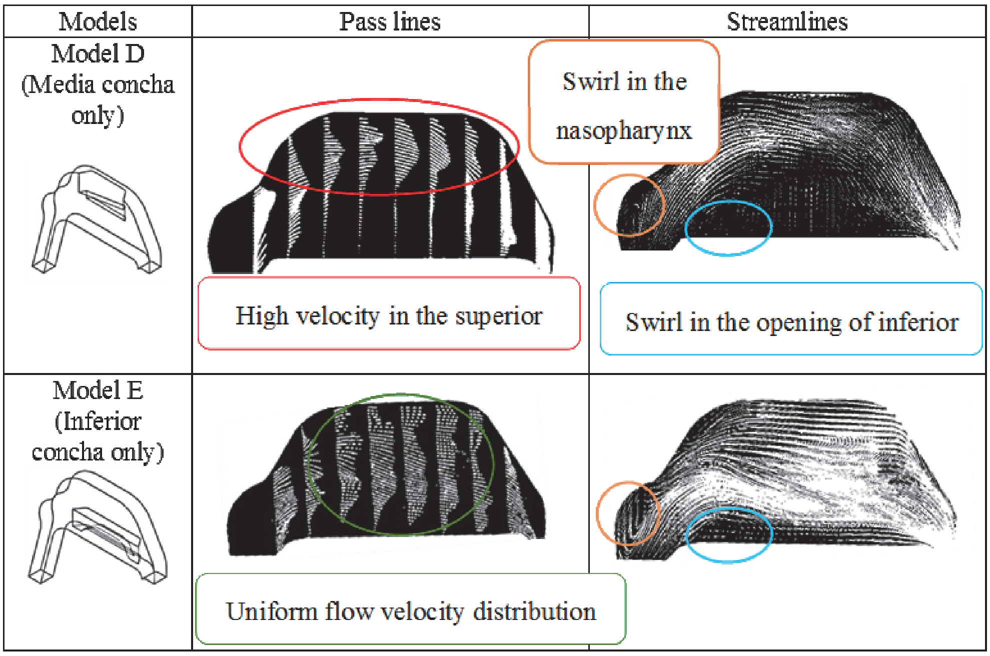

(a) Common meatus

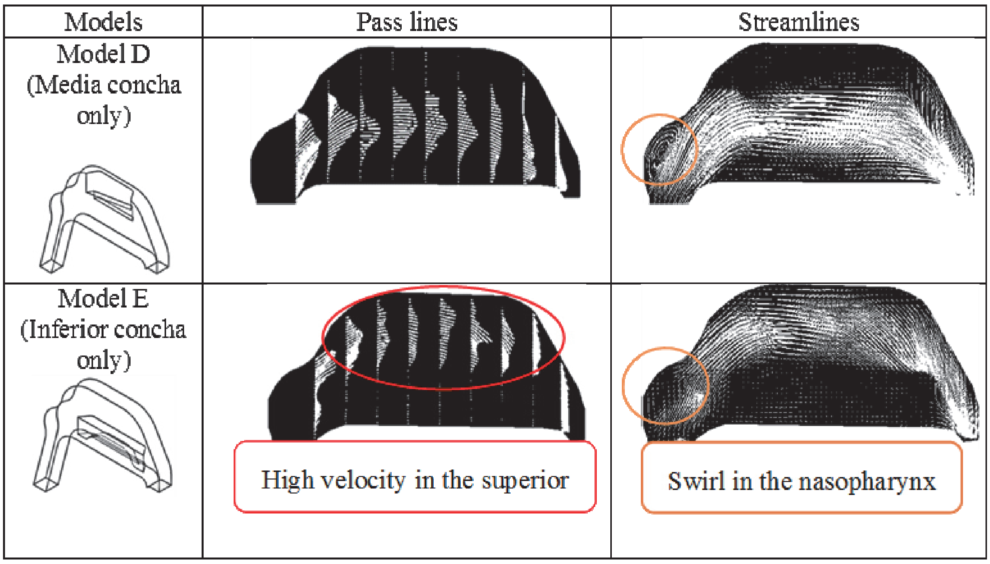

(b) Branch meatus

Fig. 12 Pass lines and streamlines during expiration

F). These effects result from the shape of nasal cavity, valve and conchae. Comparing Models B and C, higher flow rates occur in the media meatus with the presence of a longer media concha (Model B).

This occurs because the passageway abruptly narrows between the upper side of the nasal cavity and the end of the media concha, decelerating the flow along the superior meatus.

The absence of the inferior concha in Model D causes a large whirl to occur in the common meatus, which also occurs in the model without any conchae (Model A), but in the branch meatus Model D leads to a flow pattern similar to that in the Model B, characterised by a high velocity in the media meatus. Thus the inferior concha makes the cross-sectional area of the common meatus smaller, which tends to suppress flow reversal, leading to the acceleration of the flows in that region. Despite the lack of a media concha in Model E, the flow pattern in the common meatus is similar to that in the models with both conchae (Models B and C), where the flow tends to distribute evenly. From the above comparisons, we infer that the role of the long media concha is to direct flow through the media meatus and that of the inferior concha is to distribute the flow uniformly in the common meatus.

The similarity between the flow fields of the anatomically realistic model and all simplified models is the occurrence of small swirls in the upper part of the nasopharynx, which can be attributed to the similarity of the geometry in this region. Model F exhibits the airflow pattern most similar to the anatomically realistic model, which is explained by the dominant flow path being located in the media meatus, the absence of swirl in the anterior region, and the occurrence of swirls in the nasopharynx.

The recirculation in the olfactory area of the anatomically realistic model does not occur in the simplified models, which is likely because of the difference in geometries in the anterior and superior regions.

4.2 *Expiration*

As for inspiration, the lack of both conchae causes a large-scale whirl to occur in the middle of Model A. In contrast to inspiratory flow, however, a change in conchae length (between Models B and C) has almost no effect on the airflow pattern in expiration because the flow is close to uniform along the common meatus and passes mainly along the media meatus to the branch meatus. The nasal valve (Model F) is responsible for the low-velocity region in the superior part of the common meatus—the narrowed passageway intercepts the flow in this region. These flow dynamics would tend to prevent odors from the interior of the body being detected. There are similarities between the airflow patterns and velocity magnitude distributions of Model F and the anatomically realistic model. There are high velocities in the middle and inferior regions of the common meatus and in the media meatus, small velocities in the superior region, and the formation of small-scale swirls in the upper region near the nasopharynx and in the opening of the inferior meatus.

Even with the absence of the media concha in Model E, the airflow distributes uniformly along the common meatus in the same way as with both conchae present (Models B and C). Thus, the media concha functions as a guide plate. Models B and C exhibit different behaviour, however, in the branch meatus. Without the media concha, velocities are very small in the media and inferior meatus, as the flow tends to pass through the superior region. With the media concha only (Model D), high velocities occur in the superior region of the common meatus and the air in the branch meatus tends to flow through to the media meatus, as for inspiration. The airflow pattern in the branch meatus of Model D is same as that of Models B and C.

From the above analysis, we determine that the role of the media concha is (independent of its length), to guide the flow to the media meatus along the nasopharyngeal curvature. The role of the inferior concha is to make the flow in the common meatus uniform, and the role of the nasal valve is to reduce the flow rate in the superior part of the common meatus.

5. Conclusion

In our in vitro experiments, we found that the simplified model with a longer media concha and a nasal valve produced flow patterns most similar to those in the anatomically realistic model. We determined that the roles of the nasal structural elements are as follows:

1) The conchae act as guide plates to reduce the size of the large-scale whirl with reversed flow in the common meatus and in the branch meatus.

2) The nasal valve prevents further generation of swirls in the anterior region of the nasal cavity during inspiration, but during expiration it reduces the flow rate in the superior part of the common meatus.

3) The role of the media concha is to distribute the airflow among the three meatuses: during inspiration, a longer media concha makes the flow bypass the media meatus, while during expiration, the media concha, regardless of its length, guides the flow to the media meatus with the aid of the curved nasopharyngeal wall.

4) The inferior concha evenly distributes the flow in the common meatus.

Therefore, complicated flow phenomena within the anatomically realistic model have been elucidated with the help of simplified models.

The only discrepancy in the flow patterns between the anatomically realistic and simplified models was in the superior region of the common meatus during inspiration. In the neighbourhood of the olfactory region, recirculation occurred in the anatomically realistic model whereas it was not detected in most of the simplified models. This matter is investigated and discussed in Part II[24)]

References

1) Bachmann W, Legler U. Studies on the structure and function of the anterior section of the nose by means of luminal impressions. *Acta Oto-Laryngolica*. 73:433-42. 1972

2) Carlos E, Nazareth N, Josiane F, Olavo M, Jodo F. Nasal Valve: anatomy and physiology. *Brazilian Journal of Otorhinolaryngology* 75(2), 2009.

3) Afiza E, Kurashina Y, Takakura Y, Atsumi T, and Iida M. Investigation of airflow patterns within real and simplified models of nasal cavities, *The 12th International Symposium on Fluid Control, Measurement and Visualization, FLUCOME*, 2013.

4) Kastl KG, Rettinger G, Keck T. The impact of nasal surgery on air-conditioning of the nasal airways. *Thinology*. 47(3):237-241, 2009.

5) I. Horschler, C. Brucker, W. Schroder, and M. Meinke, Investigation of the impact of the Geometry on the nose flow, *European Journal of Mechanics B*, vol. 25, no. 4, pp. 471-490, 2006.

6) S. K. Chung, S. K. Kim, Digital particle image velocimetry studies of nasal airflow. *Respiratory Physiology & Neurobiology* 163, 111-120, 2008.

7) D.I. Hahn, P.W. Scherer, and M.M. Mozell, Velocity Profiles Measured for Air-flow through a Large Scale Model of the Human Nasal Cavity, *J Appl Physiol* 75: 2273-2287, 1993.

8) Churchill, S.E., Shackelford, L.L., Georgi, J.N., Black, M.T., Morphological Variation and airflow dynamics in the human nose. *Am. J. Biol.* 16, 625-638, 2004.

9) G.J.M. Garcia, G. Mitchell, N. Bailie, D. Thornhill, J. Watterson, and J.S. Kimbell, Visualization of Nasal Airflow in a Patient Affected with Atrophic Rhinitis Using Particle Image Velocimetry, *Third International Conference on Optical and Laser Diagnostic*, 2007

10) Hopkins LM, Kelly JT, Prasad AK, and Wexter AS, Particle image velocimetry measurements in complex geometries. *Exp Fluids* 29:91-95, 2000.

11) Doorly, D.J., Taylor, D.J., Gambarutto, A.M., Schroter, R.C., Tolley, N., 2008b. Nasal architecture: form and flow. *Philos. Trans. R. Soc. A* 366, 3255-3246, dio:10.1098/rsta.0083, 2008

12) D.J. Doorly, D.J. Taylor, and R.C. Schroter, Mechanics of Airflow in the Human Nasal Airways, *Respiratory Physiology & Neurobiology*, Vol. 163, pp.100-110, 2008.

13) T. Sakata, G. Tanaka, T. Sera, N. Kakusho, H. Yokota, K. Ono, and S. Takagi, Voxel Simulation of Nasal Cavity, *The Proceedings of 22nd Bioengineering Conference*, *The Japan Society of Mechanical Engineers,* 2010.

14) Keyhani, K., Scherer, P.W., Mozell, M.M. Numerical Simulation of airflow in the human nasal cavity. *J. Biomech. Eng.* 117, 429-441, 1995.

15) E.Afiza, Y.Takakura, Y. Takakura, T. Atsumi, M. Iida, On Airflow Patterns within Real and simplified models of nasal cavities (Comparison of numerical simulation with experiments). *Proceedings of the 26th Bioengineering Conference*, *The Japan Society of Mechanical Engineers,* 2014.

16) I. Horschler, M. Meike, W. Schroder, Numerical Simulation of the flow field in a model of the nasal cavity, *Computer and Fluids* 32; 39-45, 2003.

17) J. Zhang, Characteristic size research of human nasal cavity and the respiratory airflow CFD analysis, *Journal of Biosciences and Medicines, 1, 23-27*, 2013

18) C.E. Rennie, C.M. Hood, E.J.S.M. Blenke, R.S. Schroter, D.J. Doorly, et al., Physical and Computational Modeling of Ventilation of the Maxillary Sinus, *Head and Neck Surgery*, pp.164-170, 2011.

19) Y. Izumi, T.Tajikawa, K.Ohba, Y. Uesugi, In vitro experiment on reciprocating flow in a model of the nasal cavities and pharynx, *The Proceedings of the 19th Bioengineering Conference*, *The Japan Society of Mechanical Engineers,* 2007.

20) C. Suzuki, Y. Takakura, T. Atsumi, T. Takeo, M. Iida, and K. Saito, Numerical Simulation of flows in models of cavities with paranasal sinuses, *Proceedings of 2011 Annual Meeting, Japan Society of Fluid Mechanics,* 2011.

21) C. Suzuki, R. Shishido, Y. Takakura, T. Atsumi, T. Takeo, K. Saito, M. Iida, In Vitro Study of Flows in Model of Nasal Cavities with Paranasal Sinuses. *Proceedings of the 24th Bioengineering Conference*, *The Japan Society of Mechanical Engineers,* 2012.

22) E. Alias, A. Ariffin, Y. Takakura, T. Atsumi, M.Iida, Investigation of Airflow Patterns within Real and Simplified Models of Nasal cavities (Variation of Simplified models), *16th International Symposium on Flow Visualization, June 24-28*, Okinawa, 2014.

23) Y. Izumi, T.Tajikawa, K.Ohba, Y. Uesugi, In vitro experient on reciprocating flow in a model of the nasal cavities and pharynx, *The Proceedings of the 19th Bioengineering Conference*, *The Japan Society of Mechanical Engineers,* 2007.

24) E. Alias, Y. Takakura, T. Atsumi, M.Iida, Airflow pattern within Real and 3D simplified Models of Nasal Cavities (Ⅱ Numerical study), Proc. Schl. Tokai University (to appear)